Research Article | Vol. 31, No. 10 / 8 May 2023 / Optics Express 15953
Optics EXPRESS

Levitating the noise performance of ultra-stable laser cavities assisted by a deep neural network: the non-intuitive role of the mirrors

J. DICKMANN,[1,2,†*] L. SHELLING NETO,[1,2,†] M. GAEDTKE,[1,2,3] AND S. KROKER[1,2,4]

[1]Technische Universität Braunschweig, Institut für Halbleitertechnik, Hans-Sommer-Str. 66, Braunschweig 38106, Germany
[2]Laboratory for Emerging Nanometrology, Langer Kamp 6a-b, Braunschweig 38106, Germany
[3]Leibniz Universität Hannover, Welfengarten 1, Hannover 30167, Germany
[4]Physikalisch-Technische Bundesanstalt, Bundesallee 100, Braunschweig 38116, Germany
[†]The authors contributed equally to this work.
[*]j.dickmann@tu-braunschweig.de

Abstract: The most precise measurand available to science is the frequency of ultra-stable lasers. With a relative deviation of 4×10^{-17} over a wide range of measuring times between one second and 100 seconds, the smallest effects in nature can thus be made measurable. To enable cutting-edge precision, the laser frequency is stabilized to an external optical cavity. This complex optical device must be manufactured to the highest standards and shielded from environmental influences. Given this assumption, the smallest internal sources of perturbation become dominant, namely the internal noise of the optical components. In this work, we present the optimization of all relevant noise sources from all components of the frequency-stabilized laser. We discuss the correlation between each individual noise source and the different parameters of the system and discover the significance of the mirrors. The optimized laser offers a design stability of 8×10^{-18} for an operation at room temperature for measuring times between one second and 100 seconds.

1. Introduction

Lasers have evolved rapidly since Albert Einstein described the underlying principle of stimulated emission back in 1917 [1]. Today, they can be found in a wide spectrum of applications, starting from high-power lasers for material processing [2–4], to pulsed lasers to study ultrashort phenomena [5] and ultra-stable lasers for high-precision metrology [6–8]. In addition, the fact that frequency is the most accurately measurable quantity in nature [9] justifies the various applications of ultra-stable lasers. Any measurand accessible by frequency can be measured with extremely high precision by using ultra-stable lasers. Examples include applications in optical atomic clocks [10], interferometric gravitational wave detectors [11,12], tests of relativity in space [13], the use of lasers in novel radar applications [14], and deep space navigation [15]. All these applications would benefit from a further improvement of laser stability. In addition, higher stabilities will allow novel experiments to be realized, such as laboratory-scale tests of relativity [16] or the search for dark matter [17].

The stability of free-running lasers never reaches the fundamental limit. Lasers are therefore stabilized on external cavities [18]. These are optically resonant systems with very small linewidths. Currently, the most stable lasers are based on silicon cavities cooled down to 124 K, reaching a frequency stability of 4×10^{-17} in terms of modified Allan deviation over a wide range of measuring times between one second and 100 seconds [19]. The sum of all noise sources gives the stability. Figure 1 shows schematically the structure of an external cavity for the realization of ultra-stable lasers. The laser frequency (indicated in pink) is stabilized to the length of the cavity. Therefore, the distance between the two mirrors (blue) should be as

#483550 https://doi.org/10.1364/OE.483550
Journal © 2023 Received 14 Dec 2022; revised 17 Mar 2023; accepted 28 Mar 2023; published 27 Apr 2023

Optics EXPRESS

constant as possible. This is realized using a spacer (yellow), which should be shielded as well as possible from external influences. In addition, the mirrors must be of outstanding optical quality in order to achieve high cavity finesse. For this purpose, in particular the optical losses such as stray light, absorption, mode hopping and others [20] must be reduced to a minimum. In addition to external noise sources such as seismic coupling [21], temperature variations [22], or electronic noise [23], the fundamental internal noise sources limit the ultimate stability that can be achieved. These internal noise sources, in turn, are composed of many individual contributions: Each component of the cavity, especially the spacer, the mirrors, and the highly reflective mirror coatings exhibit specific noise characteristics. Since it is impossible to operate cavities at a temperature of absolute zero, the atoms in the solid move stochastically. This temperature-dependent effect is called thermo-mechanical noise (TM) [24]. In addition, local temperature fluctuations occur due to the stochastic nature of atomic motion. These lead to two different but coupled noise sources: Thermo-elastic noise (TE) [25] and thermo-refractive noise (TR) [26], which are grouped under the term thermo-optical noise (TO). Other internal noise sources are much smaller than TM and TO noise and are therefore neglected. For the sake of completeness, thermal charge carrier-driven noise [27] and photoelastic noise [28] should be mentioned. TM noise is well studied for mirrors [29], and mirror coatings [30]. However, the influence of the cavity spacer has not yet been systematically considered. In addition, to the best of our knowledge, there has been no investigation of the TO noise of spacers for ultra-stable lasers.

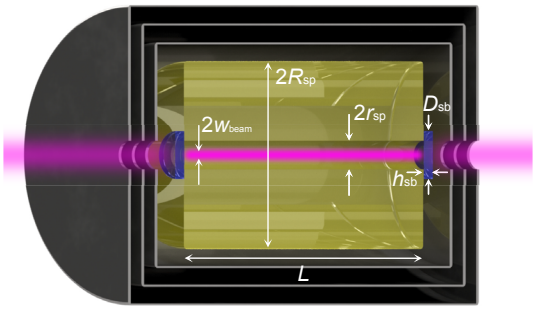

Fig. 1. Schematic representation of the ultra-stable laser cavity. The spacer (made of ULE glass) is shown as yellow glass, the mirrors (made of fused silica) as blue glass. The gray capsules represent temperature shields and vacuum recipient. All parameters important for optimization are also shown: Spacer length L, beam radius w_{beam}, spacer radius R_{sp}, bore radius r_{sp}, mirror diameter D_{sb} and mirror thickness h_{sb}.

Machine learning has evolved to a powerful tool for designing optical systems. Specifically, neural networks have been used to optimize various cavity-related applications. For example, Dai et al. designed color filters based on Fabry-Perot cavities using bidirectional neural networks [31], while Lan et al. used various neural network approaches such as tandem neural networks to design metamaterial microcavities [32]. A combination of deep neural networks and genetic algorithms was used to realize hybrid nanophotonic slit-Bragg cavities [33]. Finally, a sub-100-nW-threshold Raman silicon laser was designed by optimizing the product of cavity Q-factors with Convolutional Neural Networks [34]. In this work, a neural network was used to develop an optimization scheme allowing for a much more time efficient optimization than conventional methods. Our proposed scheme follows a carefully selected sequence of parameter optimizations to design an optical cavity minimizing all significant noise sources of all components. In this, sense our optimization scheme allowed for human supervision to ensure that the final cavity parameters obey feasible experimental boundary conditions.

Optics EXPRESS

The noise sources are introduced in the following section. In a large-scale numerical study, all six cavity parameters (see Fig. 1) are varied over a wide range and all noise sources are evaluated. This study is subject of section 3. Subsequently, the correlations between different noise sources on the cavity parameters are evaluated, see section 4. Due to the vast parameter space and the broad range of noise sources, the numerical study is time-consuming. This challenge is tackled with a deep neural network (see section 5). This network enabled the systematic optimization of all cavity parameters for minimum noise. The respective procedure is described in section 6, and the results are presented. In the last section of the results, section 7, the stabilities of the optimized cavities are compared with the world's most stable lasers.

2. Sources of thermal noise in ultra-stable lasers

It has been shown in the past that external sources of noise such as temperature fluctuations, vibrations, etc. can be effectively suppressed by suitable methods such as multi-stage temperature stabilization and vibration isolation [19,35]. The best frequency stability for a wide range of measuring times between one second and 100 seconds is limited by the fundamental noise of the cavity [19,35]. Improving the fundamental noise also leads to the need to further suppress the technical noise sources. The ultimate achievable stability limit is then given by internal noise sources, i.e., TM and TO effects. Currently, the most stable lasers are operated at cryogenic temperatures (T=124 K) and achieve a frequency stability of 4×10^{-17} [19], which is limited by the TM noise of the mirror coatings. The spacer of this device is made of monocrystalline silicon with a length of 21 cm. Both framework conditions, i.e., operation at cryogenic temperature and expensive high-quality spacer material, make accessibility considerably more difficult. More easily accessible are ultra-stable systems at room temperature. Currently, the most stable room temperature laser has a frequency stability of 8×10^{-17} [35], which is only a factor of two worse than its cryogenic counterpart. The spacer, in this case, is made of ultra-low expansion glass (ULE), which is more available and cost-efficient than monocrystalline silicon. For this reason, the following noise calculations are carried out for ULE and silicon.

We calculate the noise of the individual components as the noise power density [36] of the spatial fluctuations $S_{\mathrm{L}}(f)$ with the unit m^2/Hz. This quantity expresses how much the effective cavity length fluctuates at a specific observation frequency f with a bandwidth of 1 Hz. At the end of this section, when all noise terms are determined, this quantity is converted into Modified Allan Deviation. In general, thermal noise can be calculated using the fluctuation-dissipation theorem (FDT) [37], which establishes the relationship between spontaneous fluctuations of a system at equilibrium (noise) and the response of the system to external disturbances. Since it is substantially easier to compute the latter, the FDT provides an effective and robust approach for computing internal noise sources [38]:

$$S_{\mathrm{L}}(f) = \frac{2k_{\mathrm{B}}T}{\pi^2 f^2}\frac{W_{\mathrm{diss}}}{F_0^2}, \tag{1}$$

here k_{B} is the Boltzmann constant, T is the absolute temperature, f is the observation frequency, and W_{diss} is the dissipated power under the integrated ponderomotive pressure F_0. The TM noise is read out exclusively at surfaces. The dissipation mechanism in this case is the mechanical loss $\phi(\vec{r})$. Thus, the dissipated power is [26]:

$$W_{\mathrm{diss}}^{\mathrm{TM}} = 2\pi f \iiint_V \phi(\vec{r}) e_{\mathrm{elast}}(\vec{r}) \mathrm{d}^3 r, \tag{2}$$

where $e_{\mathrm{elast}}(\vec{r})$ denotes the elastic energy density stored in the cavity component.

For TO noise, the dissipation mechanism is thermal dissipation. The invoked thermal fluctuations lead on one hand to volume changes proportional to the thermal expansion coefficient

Optics EXPRESS

α (TE noise) and on the other hand to refractive index changes proportional to the thermo-refractive coefficient β (TR noise). In the first case, the dissipated power is [39]:

$$W_{\mathrm{diss}}^{\mathrm{TE}} = \kappa T \left(\frac{Y\alpha}{(1-2\sigma)C_{\mathrm{V}}\rho} \right)^2 \left\langle \iiint_V (\Delta\vec{u})^2 \mathrm{d}^3 r \right\rangle, \tag{3}$$

where κ is the thermal conductivity, Y the Young's modulus, σ the Poisson's ratio, C_{V} the specific heat, ρ the mass density, $\vec{u}$ the displacement field and $\langle\cdot\rangle$ is the temporal average. In the latter case (TR noise), the dissipated power is [26]:

$$W_{\mathrm{diss}}^{\mathrm{TR}} = \iiint_V \frac{\kappa}{T} \left\langle (\nabla \delta T(\vec{r}))^2 \right\rangle \mathrm{d}^3 r, \tag{4}$$

with the temperature perturbation field $\delta T(\vec{r})$.

The TO noise of the cavity component is the correlated sum of TE and TR noise. Therefore, the total TO noise may be smaller than its parts if the signs of the expansion and thermo-optical coefficients are identical [40]. In the past, it has been found that mostly TM noise from the mirror coatings dominates over all other noise sources [19]. For this reason, we pay special attention to the coatings in this work. Conventionally, the high mirror reflectivity is realized with the help of amorphous multilayer systems [41]. Due to these coatings' relatively high mechanical losses, the TM noise is also relatively high [42]. Therefore, in the following we also optimize for the use of crystalline coatings with low mechanical loss [43] as well as a novel mirror technology based on nanostructured surfaces, i.e., meta-mirrors [44,45]. Using Eqs. (1)–(4), the thermal noise of all cavity components can be calculated numerically. In the case of the spacer and the substrate, the TO noise consists exclusively of TE noise, since the light does not interact with refractive index fluctuations in the spacer and substrate (compare Fig. 1). This is described in the following section.

3. Numerical calculation of the individual noise components

The total stability of the laser is determined by the individual noise contributions of each component of the external cavity. As the previous section states, the components' noise comprises TM and TO. All noise contributions can be calculated using the fluctuation-dissipation theorem (1). Only the dissipated powers W_{diss} differ depending on the noise source and cavity component (compare Eqs. (2)–(4)). These dissipated powers were calculated numerically using the COMSOL Multiphysics software for a measuring time of one second [67]. The cylindrical symmetry of the cavity (compare Fig. 1) was exploited to perform the numerical simulation in two instead of three dimensions. This enabled a time- and energy-efficient calculation. A perfectly Gaussian intensity distribution modeled the radiation pressure on the mirror surfaces. An optically stable cavity requires at least one focusing mirror. In this analysis we have only investigated large radii of curvature >1 m, which makes the effect of mirror curvature on the noise contributions negligible. The dominant quantity in this context is the beam radii of the Gaussian beam at the mirrors. Adaptive mesh refinement ensured the convergence of the study. The area of the laser spot was given special care by logarithmic mesh refinement. Using the material parameters in Table 1, the displacement noise S_{L} was calculated for the observation frequency $f = 1$ Hz. This calculation was performed for each cavity component (spacer made from ULE, mirror made from FS, different coating types) for TM and TO noise. A parameter sweep was set up to evaluate the dependencies of the different noise contributions on the cavity parameters. In the course of this, 18,750 numerical noise calculations were performed. This corresponds to five different values for each cavity parameter: Length L (10 cm ... 50 cm), spacer radius R_{sp} (50 mm ... 250 mm), bore radius r_{sp} (2 mm ... 10 mm), mirror diameter D_{sb} (25 mm ... 75 mm), mirror thickness h_{sb} (4 mm ... 20 mm), and laser beam radius w_{beam}

Optics EXPRESS

(400 μm ... 2000 μm). Despite this vast number of time- and energy-consuming simulations, five values per parameter are far from sufficient for a reliable optimization. The computation time and energy consumption increase exponentially with the number of values per parameter. Thus, increasing this number to ten (which would still be too few for optimization) would extend the computation time to over a year. Therefore, to realize a reliable optimization, a deep neural network was trained on the simulated noise data. It can compute any noise source for any component and parameter combination with high speed and precision. In section 5, this network and its performance for optimization are presented in detail. However, before the optimization can be performed, the correlations of the noise sources with the cavity parameters should be investigated. This investigation is presented in the following section.

Table 1. Material parameters

Material Parameter	ULE Spacer	FS Substrate	SiO_2 Coating	Ta_2O_5 Coating	GaAs Coating	AlGaAs Coating	Si meta
ϕ (rad)	1×10^{-5} [46]	1×10^{-6} [47]	5×10^{-4} [48]	5×10^{-4} [48]	2.5×10^{-5} [43]	2.5×10^{-5} [43]	5×10^{-5} [49]
Y (Pa)	68×10^{9} [50]	72×10^{9} [51]	72×10^{9} [51]	140×10^{9} [52]	85.9×10^{9} [53]	84.6×10^{9} [53]	130×10^{9} [54]
σ (1)	0.17 [50]	0.17 [51]	0.17 [51]	0.23 [55]	0.31 [56]	0.35 [53]	0.28 [54]
α (1/K)	3×10^{-8} [57]	4.2×10^{-7} [58]	4.2×10^{-7} [58]	3.6×10^{-6} [59]	5.7×10^{-6} [56]	5.5×10^{-6} [53]	2.6×10^{-6} [60]
β (1/K)	-	8.5×10^{-6} [61]	8.5×10^{-6} [61]	14×10^{-6} [25]	2.4×10^{-4} [62]	2.3×10^{-4} [53]	1.8×10^{-4} [61]
κ (W/m/K)	1.31 [57]	1.4 [58]	1.4 [58]	33 [55]	55 [56]	9.88 [53]	142 [63]
C_V (J/kg/K)	767 [57]	765 [58]	765 [58]	306 [64]	327 [56]	378 [53]	711 [65]
ρ (Kg/m^3)	2210 [57]	2210 [58]	2210 [58]	6850 [52]	5317 [56]	4696 [53]	2329 [66]

4. Correlation analysis of all geometry parameters

Since the optimization of the ultra-stable laser is a high-dimensional problem (six different input parameters and six different output noise variables as well as the three different coating types), we should have an overview of the influence of the different parameters on the different noise sources. For that, the Pearson correlation matrix provides a helpful tool [68,69]. It represents the normalized covariance between the cavity parameters and the noise sources. The correlation values, termed correlation coefficients, vary between -1 and 1. The absolute value reflects the strength of the covariance and, thus the strength of the corresponding correlation. The sign indicates whether both variables grow together (positive) or not (negative). To our knowledge, this is the first systematic analysis of correlations of all major noise sources with all major parameters for ultra-stable lasers. In particular, the TM and TO noise of the cavity spacer has never been systematically considered. According to the results depicted in Fig. 2, for spacer TM noise, the spacer length (positive correlation, i.e., larger noise for larger length) and the spacer radius (negative correlation, i.e., smaller noise for larger radius) are essential. This is consistent with previous findings that examined only this correlation [8].

Surprisingly, the mirror size is clearly more important for the spacer TM noise than the spacer size itself. A large mirror thickness manifests in reduced spacer noise (TM). One possible explanation is that the transmission of spacer noise to the mirror surfaces (where the laser reads out the fluctuations) is more inefficient for thick mirrors. This intermediate result represents a paradigm shift in the design of ultra-stable lasers, as it opens a new dimension of noise optimization. This correlation may explain the experimentally observed reduction of the spacer noise when using ULE compensation rings on the mirror substrates [70]: These rings increase the effective mirror thickness and thus reduce the spacer noise (see Fig. 2).

Optics EXPRESS

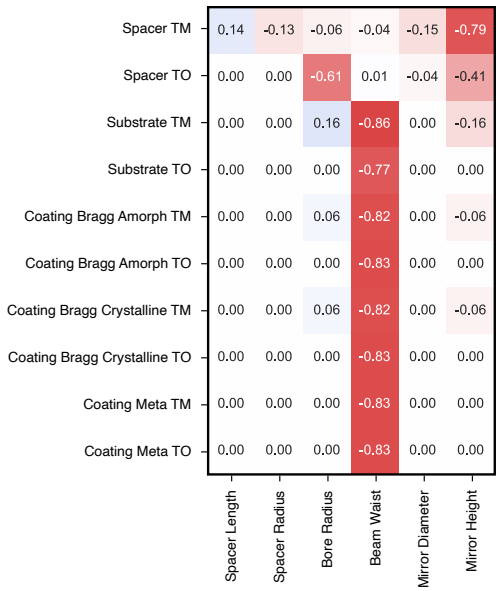

Fig. 2. Pearson correlation matrix of noise sources and all relevant cavity parameters. Compare Fig. 1 for the representation of all cavity parameters. Large absolute values close to 1 (-1) indicate strong correlation (anti-correlation).

To our knowledge, TO spacer noise has never been investigated before. For this noise source, the correlation matrix (Fig. 2) shows a clear covariance with the bore radius (the larger, the smaller the noise) and again with the mirror thickness (which should also be maximized). In the case of TM substrate noise, which is well studied due to its importance in interferometric gravitational wave detectors [29], a large laser beam radius is particularly helpful. A weak correlation between the bore radius and the mirror thickness is also noticeable. For all other noise sources, i.e. substrate TO noise as well as TO and TM noise of the mirror coatings (for all coating technologies), only the laser beam radius is important. Again, a large laser beam provides low noise because it averages over a larger (uniformly fluctuating) surface area. In particular, a large laser beam reduces many noise sources without increasing a single one. Furthermore, thick mirrors are advantageous. The only parameter that shows opposite covariances with different noise sources is the bore radius, which must be optimized for spacer TO and substrate TM noise. After this qualitative analysis of the numerically generated thermal noise data, the quantitative optimization of all cavity parameters can now be performed. For this purpose, the neural network described in the next section is used. The optimization results can be found in section 6.

5. Deep neural network for minimizing noise

A parameter sweep that covers six parameters with appropriately small step sizes takes much time, considering the computational scope of one simulation carried out by finite-element method. As a much more efficient alternative, we utilized a data-driven deep neural network that is trained on a relatively small number of simulated samples. The ten noise contributions of 18,750 samples that each share the same six input parameters were horizontally concatenated into one data set. This data set was separated into a training, validation and test set of 72 %, 18 %, and 10 %, respectively. The network architecture consists of six fully connected layers where the number of neurons is halved with each subsequent layer, starting at 1024. Each layer uses the Leaky ReLU activation function ($\alpha = 0.3$) with a sigmoid activation in the regression layer. We chose Adam [71] as an

Optics EXPRESS

optimizer with a learning rate of 0.001 and a decay value of 0.005. After 500 epochs, the network reached an MSE error of 2.15×10^{-6} and an R^2-score of 0.99991 on the test set. Now, we can decrease the time for obtaining the thermal noise for one parameter combination by a factor of 36 from 2 s to only 55 ms. In addition, the matrix-based nature of a neural network allows the prediction of multiple parameter combinations to be scaled without significant computational overhead. The network is able to understand the underlying information from the dataset to predict the noise for every parameter combination with excellent performance.

6. Optimization of all parameters

The cavity length L is set as the starting point of the optimization. The correlation matrix (Fig. 2) shows that L only influences the spacer TM noise. That means shorter cavities tend to generate less noise. Nevertheless, we set the cavity length to $L = 48$ cm. We do this for two reasons: 1. the stabilizability of a laser to a cavity depends not only on the noise but also on purely optical quantities such as the mirror reflectivity and the cavity length [72]. A 48 cm long cavity can be stabilized well [35]; 2. the currently most stable room temperature cavity also has a length of 48 cm [35]. Thus, the choice of this length enables direct comparison and validity check to the best stabilities achieved so far.

Next, the spacer radius is considered. According to Fig. 2, it exclusively influences spacer TM noise. The spacer radius is decisive for the size of the periphery (temperature stabilization and vacuum systems) and thus plays a critical role in practical implementation. As illustrated in Fig. 2, spacer TM noise also depends on other parameters, such as for example, mirror diameter and mirror height. For a first illustration of the spacer radius' influence on TM noise, Fig. 3 is based on a set of these parameters that is optimized for a minimum TM noise. For this optimization, crystalline mirrors were considered. The negative slope corresponding to its correlation coefficient in Fig. 2 can be seen. In addition, the noise converges above a certain spacer radius. Considering a threshold of 10 % above the noise minimum value, we have set this to $R_{\mathrm{sp}} = 96.3$ mm.

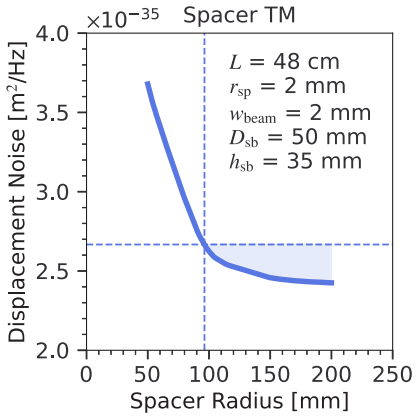

Fig. 3. Spacer radius optimization. Spacer TM noise in terms of displacement noise spectral density versus spacer radius in mm. All other parameters are taken from the optimization for crystalline coatings. That is, the spacer length L, bore radius r_{sp}, beam waist w_{beam}, mirror diameter D_{sb} and mirror thickness h_{sb}.

The remaining correlations for spacer TM noise, namely mirror height and mirror diameter, are shown in Fig. 4(a). The dashed line outlines the area of less than a 10 % increase from the noise minimum for the already defined parameters $L = 48$ cm and $R_{\mathrm{sp}} = 96.3$ mm. The indicated area shows that a mirror diameter larger than 35 mm and a mirror height of approximately 10 mm

Optics EXPRESS

to 45 mm lead to optimized spacer TM noise. In particular, the mirror height is also important for spacer TO noise. Figure 4(b) shows the spacer TO noise as a function of the mirror thickness and the bore radius. This noise contribution is three orders of magnitude below the spacer TM noise. Therefore, we have defined a threshold of 200 % for the optimization. The optimized area (dashed line) was supplemented by the already evaluated limits of the mirror height of the spacer TM noise (dashed area). This results in the shaded area for mirror height and bore radius in Fig. 4(b).

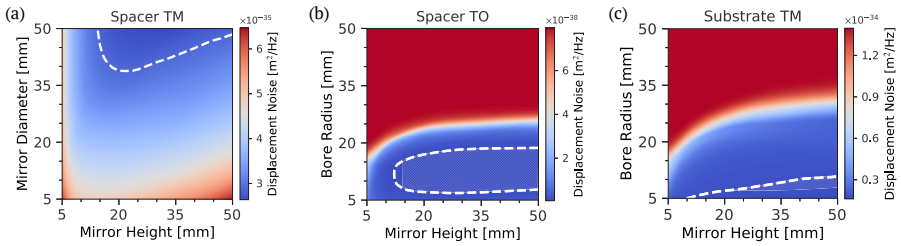

Fig. 4. Mirror height and bore radius optimization. (a) Spacer TM noise in terms of displacement noise spectral density versus mirror diameter and mirror height in mm. (b) Spacer TO noise in terms of displacement noise spectral density versus bore radius and mirror height in mm. (c) Substrate TM noise in terms of displacement noise spectral density versus bore radius and mirror height in mm. All other parameters are taken from the global optimization for crystalline coatings. The dashed areas show regions with the lowest noise after applying the findings of the preceding figure.

Besides, spacer TM noise, mirror height and bore radius are also relevant parameters for the (mirror) substrate TM noise. The beam radius can be left out at this point, since the optimized value of $w_{\mathrm{beam}} = 2000\,\mu$m does not change due to the strong covariance with the other noise sources. Overlapping the optimized (shaded) area in Fig. 4(b) and the new minimization (dashed line), results in a new area for optimizing all noise sources. This is shown hatched in Fig. 4(c).

Based on this area, the coating noise, consisting of TM and TO noise, can now be optimized. This optimization was performed for all different mirror technologies individually: Amorphous Bragg coatings, crystalline Bragg coatings and meta-mirrors. The results are shown in Fig. 5 as the dependence of coating noise on bore radius and mirror height for the parameter space of optimized spacer and substrate noise. For each individual mirror technology, the coating noise hardly varies. However, the individual coating noises differ from each other: Amorphous Bragg mirrors and meta-mirrors differ by a factor of three, which agrees with current literature, where only a single parameter set has been considered [44]. Crystalline coatings are in between the two matching to experimental findings on a respective cavity [43].

Thus, for all three mirror technologies we find the optimized parameters for maximum laser stability: $R_{\mathrm{sp}} = 96.3\,$mm, $w_{\mathrm{beam}} = 2000\,\mu$m, $r_{\mathrm{sp}} = 7.5\,$mm, $D_{\mathrm{sb}} = 50\,$mm, $h_{\mathrm{sb}} = 30\,$mm. The neural network can also be quickly and efficiently used for future optimization tasks with specific requirements to the geometry, e.g., shorter cavities or limited space. For the final design of a cavity, the vibration sensitivity must be optimized for the targeted measuring frequency spectrum. In addition, appropriate mounts, vibration isolation and temperature stabilization must be considered.

Optics EXPRESS

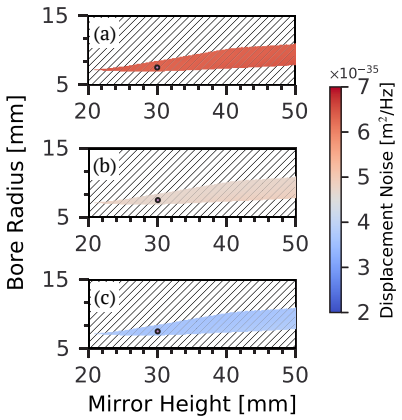

Fig. 5. Final optimization of bore radius and mirror height for all coating types. Total coating noise in terms of displacement noise spectral density versus bore radius and mirror height in mm. All other parameters are taken from the global optimization. (a) Amorphous Bragg mirror, (b) crystalline Bragg mirror, and (c) silicon meta-mirror.

7. Stability comparison of ultra-stable lasers

Now that all cavity parameters have been optimized, the total noise of the ultra-stable laser can be calculated. Figure 6 shows all noise sources of all cavity components for the three different (mirror) coating technologies. Additionally, the noise components of the currently most stable laser at room temperature have been added for comparison [35]. The TO noise is negligible in all cases and for all components. Nevertheless, it is useful to consider it in future studies, since it can become larger at cryogenic temperatures, for example. Compared to [35], each noise component can be significantly reduced: The spacer TM noise and the substrate TM noise each by a factor of 3, and the coating TM noise for amorphous Bragg mirrors by more than an order of magnitude.

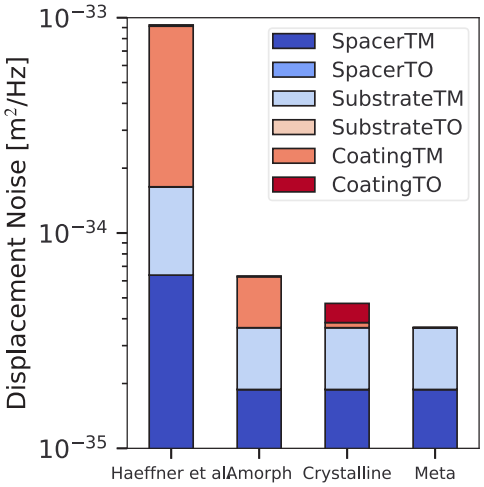

Fig. 6. Total noise, which indicates the stability of the system for a measuring time of one second. Uncorrelated sum of all noise sources of all cavity components. Shown is the noise of the current laser with the highest stability at room temperature by Haefner et al. [35] and the noise of the cavities optimized in this work for the different mirror technologies: Amorphous Bragg coatings, crystalline Bragg coatings and meta-mirrors.

Optics EXPRESS

In sum, the frequency stability of the laser can be improved by 74 % only by changing the cavity geometry. Thus, this room-temperature cavity could already surpass the most stable lasers in the world, which so far have to be operated at cryogenic temperatures [19,73]. By replacing the amorphous coatings with crystalline mirrors, a 77 % improvement in frequency stability is possible. In the case of meta-mirrors, the coating noise becomes negligible, and the stability of the laser is limited only by spacer noise. The determined frequency stability for this case is 8×10^{-18} in terms of modified Allan deviation for a measuring time of one second, which would outperform the world's most stable lasers by 80 %. The comparison of the optimized cavity geometry with the current one is shown in Fig. 7. The larger spacer radius and the larger mirrors are particularly striking.

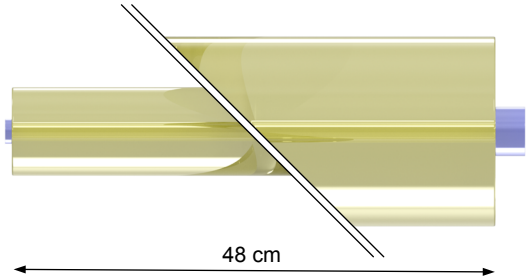

Fig. 7. Comparison of the current most stable room temperature cavity (left part) and the optimized one (right part). In particular, the larger spacer radius and the larger mirrors are striking. The right cavity shows noise reduced by an order of magnitude.

8. Conclusion

In a large-scale numerical study, we have analyzed for the first time all major noise sources in ultra-stable lasers. In addition to the thermo-mechanical noise of the cavity-spacer, the mirror substrates and the mirror layers, thermo-refractive and thermo-elastic components were also considered. These calculations were performed for the three main mirror coating technologies: Amorphous Bragg mirrors, crystalline Bragg mirrors, and meta-mirrors. By sweeping all parameters, correlations between the parameters and the noise sources were identified. A deep neural network was set up and trained on the computed data to further analyze these dependencies. This network is able to compute all noise contributions quickly and accurately for arbitrary parameter combinations. It thus provides a suitable tool to also quantitatively optimize the parameters by minimizing all noise sources. We emphasize that the optimization results are in agreement with data from previous works which only addressed single parameters at a time. The optimization yields a cavity geometry characterized in particular by a larger spacer radius and larger mirrors (compare Fig. 7). An analysis of all noise sources shows a drastically improved frequency stability of the ultra-stable laser holding the promise to outperform cryogenically operating systems already at room temperature with potential applications in gravitational wave detection, dark matter searches, and laboratory-scale tests of fundamental physics.

Funding. European Association of National Metrology Institutes (20FUN08, NEXTLASERS); Deutsche Forschungsgemeinschaft (390837967, EXC-2123, QuantumFrontiers).

Disclosures. The authors declare no conflicts of interest.

Data Availability. Data underlying the results presented in this paper are not publicly available at this time but may be obtained from the authors upon reasonable request.

References

1. A. Einstein, "Zur quantentheorie der strahlung," Physikalische Zeitschrift **18**, 121–128 (1917).

Optics EXPRESS

2. J. Powell, *CO2 Laser Cutting* (Springer, 1993).
3. C. Y. Yap, C. K. Chua, Z. L. Dong, Z. H. Liu, D. Q. Zhang, L. E. Loh, and S. L. Sing, "Review of selective laser melting: Materials and applications," Appl. Phys. Rev. **2**(4), 041101 (2015).
4. W. M. Steen and J. Mazumder, *Laser Material Processing* (Springer, 2010).
5. J.-C. Diels and W. Rudolph, *Ultrashort Laser Pulse Phenomena* (Academic Press of Elsevier, 2006).
6. T. Udem, R. Holzwarth, and T. W. Hänsch, "Optical frequency metrology," Nature **416**(6877), 233–237 (2002).
7. F. Riehle, *Frequency Standards* (WILEY-VCH, 2004).
8. T. Kessler, T. Legero, and U. Sterr, "Thermal noise in optical cavities revisited," J. Opt. Soc. Am. B **29**(1), 178–184 (2012).
9. T. W. Hänsch, "Nobel lecture: Passion for precision," Rev. Mod. Phys. **78**(4), 1297–1309 (2006).
10. A. D. Ludlow, M. M. Boyd, J. Ye, E. Peik, and P. O. Schmidt, "Optical atomic clocks," Rev. Mod. Phys. **87**(2), 637–701 (2015).
11. T. L. S. Collaboration, "Advanced ligo," Classical Quantum Gravity **32**(7), 074001 (2015).
12. K. Danzmann and L. S. Team, "Lisa: laser interferometer space antenna for gravitational wave measurements," Classical Quantum Gravity **13**(11A), A247–A250 (1996).
13. N. Gürlebeck, L. Wörner, T. Schuldt, K. Döringshoff, K. Gaul, D. Gerardi, A. Grenzebach, N. Jha, E. Kovalchuk, A. Resch, T. Wendrich, R. Berger, S. Herrmann, U. Johann, M. Krutzik, A. Peters, E. M. Rasel, and C. Braxmaier, "Boost: A satellite mission to test lorentz invariance using high-performance optical frequency references," Phys. Rev. D **97**(12), 124051 (2018).
14. U. Wandinger, *Raman Lidar* (Springer, 2005), pp. 241–271.
15. H. Hemmati, *Deep Space Optical Communications* (WILEY-INTERSCIENCE, 2006).
16. A. Tartaglia, A. D. Virgilio, J. Belfi, N. Beverini, and M. L. Ruggiero, "Testing general relativity by means of ring lasers," Eur. Phys. J. Plus **132**(2), 73 (2017).
17. E. Savalle, A. Hees, F. Frank, E. Cantin, P.-E. Pottie, B. M. Roberts, L. Cros, B. T. McAllister, and P. Wolf, "Searching for dark matter with an optical cavity and an unequal-delay interferometer," Phys. Rev. Lett. **126**(5), 051301 (2021).
18. R. W. P. Drever, J. L. Hall, F. V. Kowalski, J. Hough, G. M. Ford, A. J. Munley, and H. Ward, "Laser phase and frequency stabilization using an optical resonator," Appl. Phys. B **31**(2), 97–105 (1983).
19. D. Matei, T. Legero, S. Häfner, C. Grebing, R. Weyrich, W. Zhang, L. Sonderhouse, J. Robinson, J. Ye, F. Riehle, and U. Sterr, "1.5 μm lasers with sub 10 mhz linewidth," Phys. Rev. Lett. **118**(26), 263202 (2017).
20. E. Ronnekleiv, M. N. Zervas, and J. T. Kringlebotn, "Modeling of polarization-mode competition in fiber dfb lasers," IEEE J. Quantum Electron. **34**(9), 1559–1569 (1998).
21. J. Millo, D. V. Magalhaes, C. Mandache, Y. Le Coq, E. M. L. English, P. G. Westergaard, J. Lodewyck, S. Bize, P. Lemonde, and G. Santarelli, "Ultrastable lasers based on vibration insensitive cavities," Phys. Rev. A **79**(5), 053829 (2009).
22. M. Pizzocaro, D. Calonico, C. Calosso, C. Clivati, G. A. Costanzo, F. Levi, and A. Mura, "Active disturbance rejection control of temperature for ultrastable optical cavities," IEEE Trans Ultrason Ferroelectr Freq Control. **60**(2), 273–280 (2013).
23. T. T.-Y. Lam, B. J. J. Slagmolen, J. H. Chow, I. C. M. Littler, D. E. McClelland, and D. A. Shaddock, "Digital laser frequency stabilization using an optical cavity," IEEE J. Quantum Electron. **46**(8), 1178–1183 (2010).
24. S. A. Webster, M. Oxborrow, S. Pugla, J. Millo, and P. Gill, "Thermal-noise-limited optical cavity," Phys. Rev. A **77**(3), 033847 (2008).
25. M. Evans, S. Ballmer, M. Fejer, P. Fritschel, G. Harry, and G. Ogin, "Thermo-optic noise in coated mirrors for high-precision optical measurements," Phys. Rev. D **78**(10), 102003 (2008).
26. Y. Levin, "Fluctuation–dissipation theorem for thermo-refractive noise," Phys. Lett. A **372**(12), 1941–1944 (2008).
27. F. Bruns, S. P. Vyatchanin, J. Dickmann, R. Glaser, D. Heinert, R. Nawrodt, and S. Kroker, "Thermal charge carrier driven noise in transmissive semiconductor optics," Phys. Rev. D **102**(2), 022006 (2020).
28. J. Meyer, W. Dickmann, S. Kroker, M. Gaedtke, and J. Dickmann, "Thermally induced refractive index fluctuations in transmissive optical components and their influence on the sensitivity of einstein telescope," Classical Quantum Gravity **39**(13), 135001 (2022).
29. F. Bondu, P. Hello, and J.-Y. Vinet, "Thermal noise in mirrors of interferometric gravitational wave antennas," Phys. Lett. A **246**(3-4), 227–236 (1998).
30. G. Harry, T. P. Bodiya, and R. DeSalvo, *Optical Coatings and Thermal Noise in Precision Measurement* (Cambridge University, 2012).
31. P. Dai, Y. Wang, Y. Hu, C. H. De Groot, O. Muskens, H. Duan, and R. Huang, "Accurate inverse design of fabry–perot-cavity- based color filters far beyond srgb via a bidirectional artificial neural network," Photonics Res. **9**(5), B236–B246 (2021).
32. G. Lan, Y. Wang, and J.-Y. Ou, "Optimization of metamaterials and metamaterial-microcavity based on deep neural networks," Nanoscale Adv. **4**(23), 5137–5143 (2022).
33. J. Guimbao, L. Sanchis, L. Weituschat, J. Manuel Llorens, M. Song, J. Cardenas, and P. Aitor Postigo, "Numerical optimization of a nanophotonic cavity by machine learning for near-unity photon indistinguishability at room temperature," ACS Photonics **9**(6), 1926–1935 (2022).

Optics EXPRESS

34. T. Kawakatsu, T. Asano, S. Noda, and Y. Takahashi, "Sub-100-nw-threshold raman silicon laser designed by a machine-learning method that optimizes the product of the cavity q-factors," Opt. Express **29**(11), 17053–17068 (2021).
35. S. Häfner, S. Falke, C. Grebing, S. Vogt, T. Legero, M. Merimaa, C. Lisdat, and U. Sterr, "8×10^{-17} fractional laser frequency instability with a long room-temperature cavity," Opt. Lett. **40**(9), 2112–2115 (2015).
36. J. C. Whitaker, *The Electronics Handbook* (CRC, 2018).
37. R. Kubo, "The fluctuation-dissipation theorem," Rep. Prog. Phys. **29**(1), 255–284 (1966).
38. Y. Levin, "Internal thermal noise in the LIGO test masses: A direct approach," Phys. Rev. D **57**(2), 659–663 (1998).
39. Y. T. Liu and K. S. Thorne, "Thermoelastic noise and homogeneous thermal noise in finite sized gravitational-wave test masses," Phys. Rev. D **62**(12), 122002 (2000).
40. C. Panuski, J. Goldstein, D. Englund, and R. Hamerly, "Coherent thermo-optic noise cancellation in an optical microcavity," *Frontiers in Optics* (2021).
41. C. J. R. Sheppard, "Approximate calculation of the reflection coefficient from a stratified medium," Pure Appl. Opt. **4**(5), 665–669 (1995).
42. S. D. Penn, P. H. Sneddon, H. Armandula, J. C. Betzwieser, G. Cagnoli, J. Camp, D. R. M. Crooks, M. M. Fejer, A. M. Gretarsson, J. Harry, G. M. Hough, S. E. Kittelberger, M. J. Mortonson, R. Route, S. Rowan, and C. C. Vassiliou, "Mechanical loss in tantala/silica dielectric mirror coatings," Classical Quantum Gravity **20**(13), 2917–2928 (2003).
43. G. D. Cole, W. Zhang, M. J. Martin, J. Ye, and M. Aspelmeyer, "Tenfold reduction of brownian noise in high-reflectivity optical coatings," Nat. Photonics **7**(8), 644–650 (2013).
44. J. Dickmann and S. Kroker, "Highly reflective low-noise etalon-based meta-mirror," Phys. Rev. D **98**(8), 082003 (2018).
45. J. Dickmann, S. Sauer, J. Meyer, M. Gaedtke, T. Siefke, U. Brückner, J. Plentz, and S. Kroker, "Experimental realization of a 12,000-finesse laser cavity based on a low-noise microstructured mirror," Commun. Phys. **6**(1), 16 (2023).
46. K. Numata, A. Kemery, and J. Camp, "Thermal-noise limit in the frequency stabilization of lasers with rigid cavities," Phys. Rev. Lett. **93**(25), 250602 (2004).
47. K. Numata, G. B. Bianc, N. Ohishi, A. Sekiya, S. Otsuka, K. Kawabe, M. Ando, and K. Tsubono, "Measurement of the intrinsic mechanical loss of low-loss samples using a nodal support," Phys. Lett. A **276**(1-4), 37–46 (2000).
48. K. Yamamoto, S. Miyoki, T. Uchiyama, H. Ishitsuka, M. Ohashi, K. Kuroda, T. Tomaru, N. Sato, T. Suzuki, T. Haruyama, A. Yamamoto, T. Shintomi, K. Numata, K. Waseda, K. Ito, and K. Watanabe, "Measurement of the mechanical loss of a cooled reflective coating for gravitational wave detection," Phys. Rev. D **74**(2), 022002 (2006).
49. R. Nawrodt, C. Schwarz, S. Kroker, I. W. Martin, R. Bassiri, F. Brückner, L. Cunningham, G. D. Hammond, D. Heinert, J. Hough, T. Käsebier, E.-B. Kley, R. Neubert, S. Reid, S. Rowan, P. Seidel, and A. Tünnermann, "Investigation of mechanical losses of thin silicon flexures at low temperatures," Classical Quantum Gravity **30**(11), 115008 (2013).
50. P. Klocek, *Handbook of Infrared Optical Materials* (CRC, 2019).
51. S. Musikant, *Optical Materials: An Introduction to Selection and Application* (CRC, 2020).
52. P. Martin, A. Bendavid, M. Swain, R. Netterfield, T. Kinder, W. Sainty, and D. Drage, "Mechanical and optical properties of the films of tantalum oxide deposited by ion-assisted deposition," Symp. M1 - Thin Films: Stress. Mech. Prop. IV **308**, 583 (1993).
53. B. Guha, S. Mariani, G. Leo, I. Favero, and A. Lemaitre, "High frequency optomechanical disk resonators in iii-v ternary semiconductors," Opt. Express **25**(20), 24639 (2017).
54. M. A. Hopcroft, W. D. Nix, and T. W. Kenny, "What is the young's modulus of silicon?" J. Microelectromech. Syst. **19**(2), 229–238 (2010).
55. M. M. Fejer, S. Rowan, G. Cagnoli, D. R. M. Crooks, A. Gretarsson, G. M. Harry, J. Hough, S. D. Penn, P. H. Sneddon, and S. P. Vyatchanin, "Thermoelastic dissipation in inhomogeneous media: loss measurements and displacement noise in coated test masses for interferometric gravitational wave detectors," Phys. Rev. D **70**(8), 082003 (2004).
56. J. S. Blakemore, "Semiconducting and other major properties of gallium arsenide," J. Appl. Phys. **53**(10), R123–R181 (1982).
57. "Corning ultra low expansion glass: Advanced optics and materials," www.corning.com. 2016.
58. M. N. Waynant and R. W. Ediger, *Electro-Optics Handbook* (McGraw-Hill, Inc., 2000).
59. C.-L. Tien, C.-C. Lee, K.-P. Chuang, and C.-C. Jaing, "Simultaneous determination of the thermal expansion coefficient and the elastic modulus of ta2o5 thin film using phase shifting interferometry," J. Mod. Opt. **47**(10), 1681–1691 (2009).
60. K. G. Lyon, G. L. Salinger, and C. A. Swenson, "Linear thermal expansion measurements on silicon from 6 to 340 k," J. Appl. Phys. **48**(3), 865–868 (1977).
61. J. Komma, C. Schwarz, G. Hofmann, D. Heinert, and R. Nawrodt, "Thermo-optic coefficient of silicon at 1550 nm and cryogenic temperatures," Appl. Phys. Lett. **101**(4), 041905 (2012).
62. F. G. Della Corte, G. Cocorullo, M. Iodice, and I. Rendina, "Temperature dependence of the thermo-optic coefficient of inp, gaas, and sic from room temperature to 600 k at the wavelength of 1.5 μm," Appl. Phys. Lett. **77**(11), 1614–1616 (2000).
63. H. R. Shanks, P. D. Maycock, P. H. Sidles, and G. C. Danielson, "Thermal conductivity of silicon from 300 to 1400 k," Phys. Rev. **130**(5), 1743–1748 (1963).

Optics EXPRESS

64. G. V. Samsonov, *The Oxide Handbook* (Springer, 1973).
65. H. Abe, H. Kato, and T. Baba, "Specific heat capacity measurement of single-crystalline silicon as new reference material," Jpn. J. Appl. Phys. **50**(11S), 11RG01 (2011).
66. I. Henins, "Precision density measurement of silicon," J. Res. Natl. Bur. Stan. Sect. A **68A**(5), 529–533 (1964).
67. "Comsol multiphysics v. 6.0silicon," www.comsol.com. COMSOL AB, Stockholm, Sweden.
68. W. Brooks, "Typical laws of heredity," Nature **15**(388), 492–495 (1877).
69. "Spss tutorials: Pearson correlation," libguides.library.kent.edu/SPSS/PearsonCorr. Accessed: 2022-08-20.
70. T. Kessler, T. Legero, and U. Sterr, "Thermal noise in optical cavities revisited," arXiv, arXiv:1111.4950 (2011).
71. D. P. Kingma and J. Ba, "Adam: A method for stochastic optimization," (2014).
72. N. Ismail, C. C. Kores, D. Geskus, and M. Pollnau, "Fabry-pérot resonator: spectral line shapes, generic and related airy distributions, linewidths, finesses, and performance at low or frequency-dependent reflectivity," Opt. Express **24**(15), 16366–16389 (2016).
73. T. Kessler, C. Hagemann, C. Grebing, T. Legero, U. Sterr, F. Riehle, M. J. Martin, L. Chen, and J. Ye, "A sub-40-mhz-linewidth laser based on a silicon single-crystal optical cavity," Nat. Photonics **6**(10), 687–692 (2012).